Material growth and device fabrication of terahertz quantum-cascade laser based on bound-to-continuum structure*

Yin Rong(尹 嵘), Wan Wen-Jian(万文坚), Zhang Zhen-Zhen(张真真),
Tan Zhi-Yong(谭智勇), and Cao Jun-Cheng(曹俊诚)†

Key Laboratory of Terahertz Solid-State Technology, Shanghai Institute of Microsystem and Information Technology, Chinese Academy of Sciences, Shanghai 200050, *China*

(Received 17 May 2014; revised manuscript received 28 May 2014; published online 10 August 2014)

The terahertz quantum-cascade laser (THz QCL) based on bound-to-continuum structure is demonstrated. The X-ray diffraction measurement of the material shows a high crystalline quality of the active region. A THz QCL device was fabricated with semi-insulating surface-plasmon waveguide. The test device is lasing at about 3 THz and operating up to 60 K. It shows a single frequency property under different drive currents and temperatures. At 9 K, the maximum output power is greater than 2 mW with a threshold current density of 159 A/cm^2.

Keywords: terahertz, quantum cascade lasers, bound-to-continuum, single mode

PACS: 42.55.Px, 61.50.cp **DOI:** 10.1088/1674-1056/23/10/104207

1. Introduction

There is a broad range of applications associated with the terahertz (THz) technology.[1,2] But it has historically been characterized by a relative lack of convenient radiation sources and detectors. The THz quantum cascade laser (QCL) is a compact and coherent source in THz region, which is a unipolar device based on inter-subband transitions in the conduction band of a specifically engineered semiconductor heterostructure. Since the first successful demonstration of the QCL emitting in the THz frequency in 2002,[3] significant improvements have been made over the past few years.[4–7] Different approaches including the structural design of the active region and the waveguide have been used.[8–10] High light power (250 mW),[9] high operating temperature (200 K),[11] and wide lasing frequency (1.2 THz–5 THz) open an extensive range of potential and promising applications in spectroscopy, imaging, and sensing. However, different applications need THz QCLs operating in specific modes. For example, we require high-power THz QCLs for imaging applications, in continuous wave (cw) mode for spectroscopy, in pulsed mode for high-speed communications, and so on. Therefore, it is absolutely essential to develop the technology of THz QCLs.

Aside from the chirped superlattice (CSL) active region of the first THz QCL, two major designs of active regions have been widely used now: bound-to-continuum (BTC) and resonant-phonon (RP) designs. For BTC structure, the lower radiative state and miniband-based depopulation remains the same, but the upper radiative state is essentially made to be a bound defect state in the minigap. The effect is that radiative transition is more diagonal in real space. The oscillator strength of the transition drops slightly, as the overlap with the miniband states drops, but the upper-state lifetime increases as non-radiative scattering is similarly reduced. The injection process also becomes more selective, as the injector states couple more strongly with the upper state than with the lower miniband. As a result, these designs displayed improved temperature and power performance compared to the CSL designs.

In this work, the gas source molecular beam epitaxy (GSMBE) technique has been used to grow the lattice matched AlGaAs/GaAs THz QCL with BTC structure. The semi-insulating surface-plasmon (SI-SP) waveguide structure is used to fabricate the laser ridge. Emission spectra under different drive currents and temperatures are measured by employing a Fourier transform spectrometer. The light power–current–voltage (*L–I–V*) curves under different temperatures are acquired by using the *I–V* measurement system and a thermopile detector. The measured results are analyzed and discussed.

2. Material growth and device processing

The layer structure of THz QCL was grown on a 2-inch (1 inch = 2.54 cm) semi-insulating GaAs substrate by using the MBE system. The element beam fluxes are controlled by

*Project supported by the National Basic Research Program of China (Grant No. 2014CB339803), the National High Technology Research and Development Program of China (Grant No. 2011AA010205), the National Natural Science Foundation of China (Grant Nos. 61131006 and 61321492), the Major National Development Project of Scientific Instrument and Equipment (Grant No. 2011YQ150021), the National Science and Technology Major Project (Grant No. 2011ZX02707), and the Major Project (Grant No. YYYJ-1123-1).

†Corresponding author. E-mail: jccao@mail.sim.ac.cn

© 2014 Chinese Physical Society and IOP Publishing Ltd

changing the source temperatures. The detailed parameters for sample GS12-234 are listed in Table 1. The THz QCL layer structure comprises a GaAs buffer layer, an etch-stop layer, a bottom contact layer, an active region (90 repeats), a top contact layer, and a low-temperature GaAs cap layer. Starting from the injection barrier, the layer sequence of one period is **3.8**/14.0/**0.6**/9.0/**0.6**/15.8/**1.5**/12.8/**1.8**/12.2/**2.0**/12.0/**2.0**/11.4/**2.7**/11.3/**3.5**/11.6 in units of nm, where the $Al_{0.15}Ga_{0.85}As$ barriers are in bold face and the underlined 12.0-nm and 11.4-nm GaAs wells are silicon doped at 1.6×10^{16} cm^{-3}. The low temperature GaAs is grown at 350 °C.

Table 1. Layer structure of the THz QCL.

Layers	Detail	Thickness
Cap layer	LT-GaAs	3.5 nm
Top contact layer	GaAs:Si	50 nm
Active region×90	18 mini-layers /period	128.6 nm×90
Bottom contact layer	GaAs:Si	700 nm
Etch-stop layer	$Al_{0.55}Ga_{0.45}As$	200 nm

We characterized the THz QCL material by high-resolution X-ray diffraction (XRD), as shown in Fig. 1. The simulated curve is acquired by using the nominal design parameters above. The material composition and deviation between the expected and the actual structure can be accurately analyzed by comparing the test curve and the simulated one. The fitting value of the thickness per period from the XRD results is 126.0 nm, which shows a period thickness of 2% lower than the nominal value. The measured curve is shifted vertically for clarity. The strongest diffraction is the GaAs substrate (004) peak, while the second strongest one is the diffraction peak of the etch-stop layer. The angular separation of the zero-order diffraction peak and the substrate GaAs peak is determined by the average Al fraction. Since the Al fraction in AlGaAs barriers of the active region is relatively low, the zero order diffraction peak cannot be distinguished from the substrate one. Moreover, there are many multi-level diffraction satellite peaks typically originated from the superlattice. They match with the simulation curve relatively well. It appears only when the periodic interface and the surface are extremely smooth. Besides the strong multi-level diffraction peaks we can also see a narrow full width at half maximum (FWHM). It means a good crystal quality and a smooth interface.

Our device was designed and fabricated with standard manufacturing techniques such as metallization, photolithography, and wet etching, and so on. Ti/Pt/Au(20/20/250 nm) by magnetron sputtering was used as the n-type Ohmic contact of the top metal electrode. The bottom metal electrode is Ge/Au/Ni/Au(13/30/33/200 nm) by electron beam evaporation. The wet etchant used was H_2SO_4:H_2O_2:H_2O in the volume ratio of 1:8:160. It etches at approximately 225 nm/min and is generally reaction-limited. After finishing the ridge waveguide structure and the upper and lower electrodes, rapid thermal annealing were executed in order to get a better alloy Ohmic contact. The annealing temperature is 390 °C and the time is 40 s. The following step is reducing the thickness of the device to about 120 μm. Finally cleavage and package are the indispensable process.

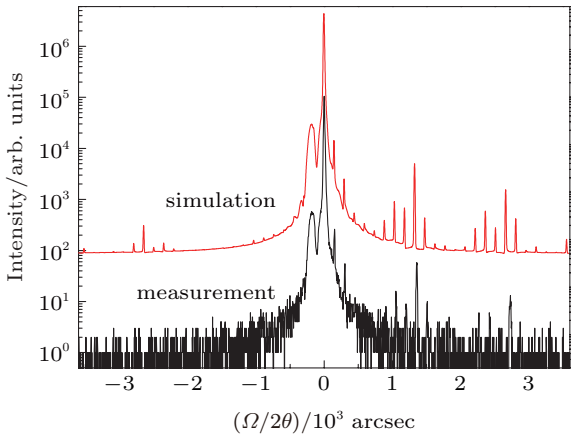


Fig. 1. (color online) XRD scan around GaAs (004) reflection.

We use the semi-insulating surface-plasmon (SI-SP) waveguide. This sort of waveguide has higher output powers and better beam patterns compared to the metal–metal (MM) waveguide. The SI-SP waveguide involves the growth of a 700-nm heavily doped layer underneath the 10-μm-thick active region, but on the top of a semi-insulating GaAs substrate. The result is a compound surface-plasmon mode bound to the top metal contact and the lower plasma layer. Although the mode extends substantially into the substrate, the overlap with any doped semiconductor is small, so that the free-carrier loss is minimized.

3. Device test and analysis

The laser was driven in pulsed mode with a 2-kHz repetition rate and a 5-μs pulse width (1% duty cycle). The laser emission was collected by a cooled Si bolometer held close to the polyethylene cryostat window. The bolometer output signal was measured with a lock-in amplifier. The current was acquired by using a current probe. To measure the output light power, the lasing emission was collected by two parabolic mirrors and focus onto a room temperature thermopile detector (Ophir 3 A-P-THz) with a measurable power range of 50 μW to 3 W.

Figure 2 shows the threshold current density J_{th} of a 180μm wide and 3mm long laser as a function of the heat sink temperature. It is evident to see that J_{th} increases with temperature, which is due to the reduction of the upper lasing level lifetime due to thermally activated LO-phonon scattering at higher temperature. In order to fit J_{th} to the empirical expression $J_{th} = J_0 + J_1 \exp(T/T_0)$, we can obtain a value of $T_0 = 27$ K, $J_0 = 144.6$ A/cm^2, and $J_1 = 7.3$ A/cm^2. At 9 K, the threshold current density is 159 A/cm^2, which is lower than all of the devices reported in Ref. [12]. The lasing continues until a current density reaches 216 A/cm^2.

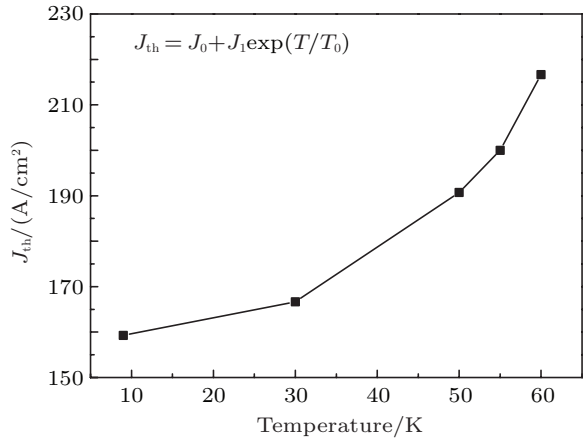


Fig. 2. J_{th} as a function of heat sink temperature.

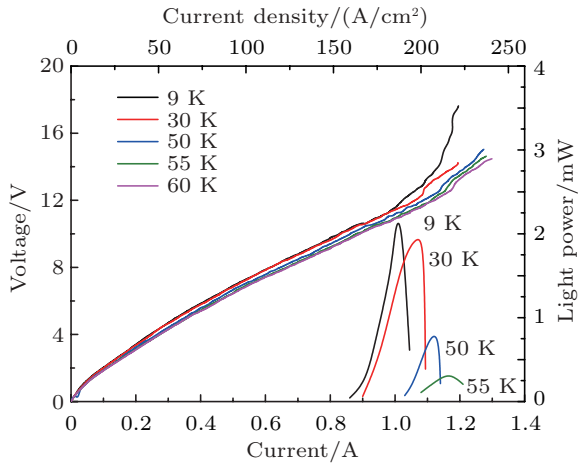


Fig. 3. (color online) *L–I–V* curves for the THz QCL device.

Figure 3 shows the light power–current–voltage (*L–I–V*) characteristics at different heat sink temperatures. Generally speaking, as the temperature increases, the resistance of the device decreases. From Fig. 3 we can see that there is a significant inflection point at the current density of about 216 A/cm^2 at 9 K. This is mainly due to the reason that the energy levels do not align well as voltage increases. As a result, the electrons cannot transport smoothly in each cycle. At 9 K, the maximum output power of the test device is more than 2 mW. And the lasing is observed up to 55 K with a power level of about 300 μW under a drive current of 1.17 A.

Figure 4 shows the typical emission spectra above threshold current at 9 K. The emission frequency is 2.99 THz, corresponding to an energy of 12.3 meV. In all the bias range, the emission is dominated by a single mode. The emission spectra under a bias of −12.34 V at different temperatures are shown in Fig. 5. For all operating temperatures, the emission frequencies of the laser always locate at 2.99 THz, which shows a good frequency stabilization with the temperature increasing. The above properties indicate that the device could be a good single frequency emitter in THz communication applications.

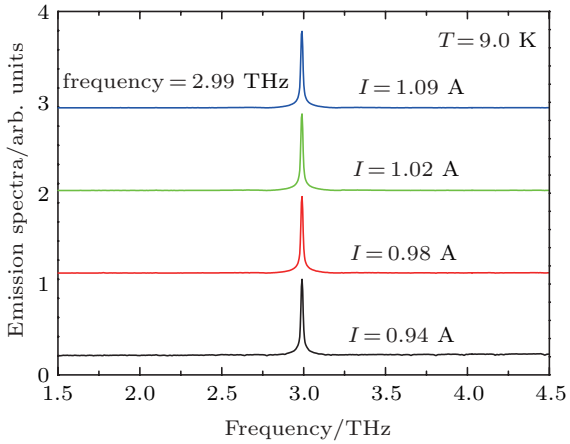


Fig. 4. (color online) The lasing spectra at $T = 9$ K.

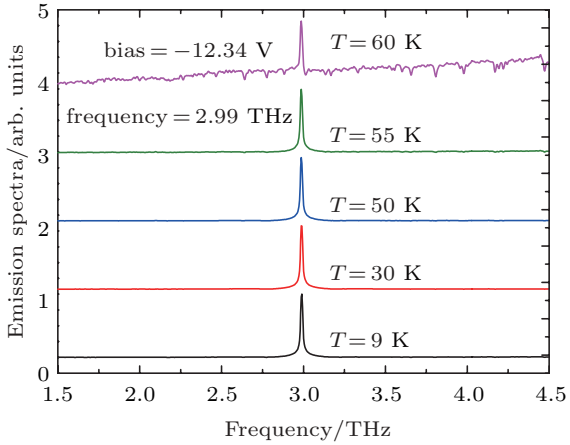


Fig. 5. (color online) Emission spectra under a bias of −12.34 V.

4. Conclusion

In this work, we have demonstrated the growth of THz QCL based on BTC structure by GSMBE. The cascade module thickness deduced from the XRD analysis shows a slight thickness deviation, with a value of inner 2%, from the nominal value, which shows a good material quality by using the

MBE method. A 180-μm-wide and 3-mm-long device is fabricated from sample GS12-234. The maximum output power is greater than 2 mW at 9 K. The lasing takes place at 2.99 THz. Though the value of T_0, with a value of 27 K, obtained by fitting $J_{\rm th}$ to the empirical expression $J_{\rm th} = J_0 + J_1 \exp(T/T_0)$ is small, the lasing is observed up to 60 K.

References

[1] Ma Y R, Guo S F and Duan S Q 2012 *Chin. Phys. B* **21** 037804

[2] Fu A B, Hao M R, Yang Y, Shen W Z and Liu H C 2013 *Chin. Phys. B* **22** 026803

[3] Kohler R, Tredicucci A, Beltram F, Beere H, Linfield E, Davies A, Ritchie D, Iotti R and Rossi F 2002 *Nature* **417** 156

[4] Darmo J, Tamosiunas V, Fasching G, Kroll J, Unterrainer K, Beck M, Giovannini M, Faist J, Kremser C and Debbage P 2004 *Opt. Express* **12** 1879

[5] Kohler R, Tredicucci A, Beltram F, Beere H E, Linfield E H, Davies A G, Ritchie D A, Dhillon S S and Sirtori C 2003 *Appl. Phys. Lett.* **82** 1518

[6] Williams B S 2007 *Nat. Photon.* **1** 517

[7] Liu H C, Wachter M, Ban D, Wasilewski Z R, Buchanan M, Aers G C, Cao J C, Feng S L, Williams B S and Hu Q 2005 *Appl. Phys. Lett.* **87** 141102

[8] Barbieri S, Alton J, Beere H E, Fowler J, Linfield E H and Ritchie D A 2004 *Appl. Phys. Lett.* **85** 1674

[9] Williams B S, Kumar S, Hu Q and Reno J L 2004 *Electron. Lett.* **40** 431

[10] Williams B S, Kumar S, Hu Q and Reno J L 2005 *Opt. Express* **13** 3331

[11] Fathololoumi S, Dupont E, Chan C W I, Wasilewski Z R, Laframboise S R, Ban D, Mátyás A, Jirauschek C, Hu Q and Liu H C 2012 *Opt. Express* **20** 3866

[12] Amanti M, Scalari G, Terazzi R, Fischer M, Beck M, Faist J, Rudra A, Gallo P and Kapon E 2009 *New J. Phys.* **11** 125022